An N4-Tetradentate Hydrazone Ligand That Binds in a Neutral, Mono- and Bisdeprotonated Form to Iron(II) and Zinc(II) Metal Ions

Pandiarajan, Devaraj ; Fox, Thomas ; Spingler, Bernhard

Abstract: The coordination chemistry of butane-2,3-dione bis (2 -pyridylhydrazone) towards the divalent first-row transition metals zinc and iron has been explored. Depending upon the conditions, the ligand in the six complexes was found to be either neutral, mono, or doubly deprotonated. The zinc(II) and iron(II) complexes were fully characterized by elemental analysis, mass spectrometry, and X-ray diffraction methods.

DOI: https://doi.org/10.3390/cryst11080982

crystals

MDPI

Article

An N4-Tetradentate Hydrazone Ligand That Binds in a Neutral, Mono- and Bisdeprotonated Form to Iron(II) and Zinc(II) Metal Ions

Devaraj Pandiarajan, Thomas Fox and Bernhard Spingler *

Department of Chemistry, University of Zürich, Winterthurerstr. 190, CH-8057 Zürich, Switzerland; michsd@gmail.com (D.P.); thomas.fox@chem.uzh.ch (T.F.)
* Correspondence: spingler@chem.uzh.ch; Tel.: +41-44-635-46-56

Abstract: The coordination chemistry of butane-2,3-dione bis (2′-pyridylhydrazone) towards the divalent first-row transition metals zinc and iron has been explored. Depending upon the conditions, the ligand in the six complexes was found to be either neutral, mono, or doubly deprotonated. The zinc(II) and iron(II) complexes were fully characterized by elemental analysis, mass spectrometry, and X-ray diffraction methods.

Keywords: crystallography; deprotonation; hydrazones; N ligands; single crystal analysis; structure elucidation; zinc

Citation: Pandiarajan, D.; Fox, T.; Spingler, B. An N4-Tetradentate Hydrazone Ligand That Binds in a Neutral, Mono- and Bisdeprotonated Form to Iron(II) and Zinc(II) Metal Ions. *Crystals* **2021**, *11*, 982. https://doi.org/10.3390/cryst11080982

Academic Editors: Miquel Barceló-Oliver and Alicia Dominguez-Martin

Received: 30 June 2021
Accepted: 17 August 2021
Published: 19 August 2021

1. Introduction

A great interest has been devoted towards the coordination chemistry of first-row transition metal complexes containing organic chelating ligands. Particularly, coordination complexes play a significant role in numerous biological functions, which has led to intensive studies in the field of bioinorganic chemistry [1–3]. Coordination compounds are fundamental in biological systems such as energy storage, oxygen transport, the proper functioning of different enzymes, electron transfer, and selective oxidation of carbon–hydrogen bonds, nitrogen fixation, and photosynthesis [4–6]. Over the past two decades, tremendous efforts have been devoted to the development of various types of supporting ligands and their metal complexes in order to model and mimic the biological systems. Iron and zinc have been found in the active sites of metalloenzymes; they catalyze a wide range of chemical reactions. Specifically, the chemistry of mono and binuclear iron(II) and zinc(II) metal complexes has aroused considerable interest in their use as model complexes as well as their biomedical applications [7–12].

Schiff bases continue to occupy an important position as ligands in metal coordination chemistry, even after more than a century since their discovery [13–19]. Schiff bases have played a key role as chelating and widely used ligands in main group and transition metal coordination chemistry due to their ease of synthesis, stability under a variety of oxidative and reductive conditions, and the structural versatility associated with their diverse applications [20–25]. A large number of Schiff bases and their metal complexes have been studied for their interesting and important properties, for example, their catalytic activity [26–32], photochromic properties [33], and use as potential antitumor drugs [34–36].

The earliest studies relevant to our work are those by Lions and co-workers, who reported the formation of cationic complexes from neutral ligands. The cationic complexes could be deprotonated, yielding neutral complexes for metals in oxidation state +II (Scheme 1) [37]. Working with butane-2,3-dione bis (2′-pyridylhydrazone), the same group described the synthesis of deprotonated complexes using 5 M sodium hydroxide [38]. Furthermore, Bailey et al. published work on the doubly deprotonated binuclear nickel complexes and their electrochemical characterization [39,40]. In 2017, Naskar et al. reported on butane-2,3-dione bis (2′-pyridylhydrazone) and hexane-3,4-dione bis (2′-pyridylhydrazone)

based copper(II) complexes [41]. Based on the very few earlier reports on the neutral N4 donor ligands and their coordination towards the transition metals, we turned our attention towards the synthesis of stable butane-2,3-dione bis (2′-pyridylhydrazone) and their coordination with zinc(II) and iron(II) metal ions in different experimental conditions. Herein, we provide a detailed description of the synthesis and structural characterization of a series of zinc(II) and iron(II) complexes with the butane-2,3-dione bis (2′-pyridylhydrazone) ligand that is either in the neutral or (bis)deprotonated form. The characterization of complexes (**1**–**6**) has been carried out on the basis of their analytic and spectroscopic parameters (see the experimental section).

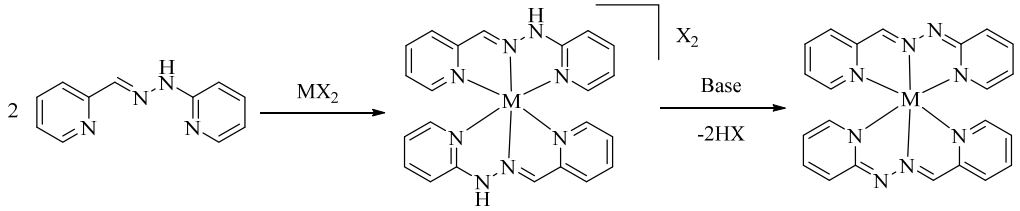

Scheme 1. Synthesis of cationic transition metal complex salts and their transformation into neutral salts [37].

2. Materials and Methods

Chemicals were purchased from ABCR GmbH (Karlsruhe, Germany), Merck KGaA (Darmstadt, Germany), or TCI-Europe N.V. (Zwijndrecht, Belgium) and used without further purification. The ligand butane-2,3-dione bis (2′-pyridylhydrazone) (**LH_2**) [41,42] and the starting precursor complexes [Fe{N(SiMe$_3$)$_2$}$_2$] [43] and [Zn{N(SiMe$_3$)$_2$}$_2$] [44] were prepared according to literature procedures. All of the reactions were performed under a nitrogen atmosphere. ESI-MS measurements were recorded on a Bruker HCT ultra mass spectrometer (Bruker Switzerland, Fällanden, Switzerland). Elemental analyses were performed on a Leco CHNS-932 elemental analyzer (Leco Instrumente GmbH, Mönchengladbach, Germany). IR spectra were recorded on a Jasco FT/IR-4200 spectrometer type A (JASCO Deutschland GmbH, Pfungstadt, Germany). NMR spectra were recorded on a Bruker 300, AV2-400, and DRX 500 MHz spectrometer (Bruker Switzerland, Fällanden, Switzerland). The chemical shifts are relative to residual solvent signals as reference. The assignment of ^{1}H- and ^{13}C-signals was made by 2D-NMR, namely COSY, HMQC, HMBC, and difference NOESY-spectrometry.

Crystallographic data were collected at 183(2) K with either Mo K$_\alpha$ radiation (λ = 0.7107 Å) or Cu K$_\alpha$ radiation (λ = 1.5418 Å). The complexes (**2**–**6**) were measured on an Rigaku SuperNova, Dual source (Rigaku Europe SE, Neu-Isenburg, Germany), with an Atlas detector, while complex **1** was measured on an Rigaku Oxford Diffraction CCD Xcalibur system with a Ruby detector (Rigaku Europe SE, Neu-Isenburg, Germany). Suitable crystals were covered with oil (Infineum V8512, formerly known as Paratone N; Infineum, Milton Hill, UK), placed on a nylon loop that was mounted in a CrystalCap Magnetic™ (Hampton Research, Aliso Viejo, CA, USA), and immediately transferred to the diffractometer. Data were corrected for Lorentz and polarization effects as well as for absorption (numerical). The program suite *CrysAlis^{Pro}* was used for data collection, multi-scan absorption correction, and data reduction [45]. Structures were solved with direct methods using *SIR97* [46] and were refined by full-matrix least-squares methods on F^2 with *SHELXL-2018* [47]. The structures were checked for higher symmetry with the help of the program *Platon* [48]. The graphical output was produced with the help of the program *Mercury* [49]. Further crystallographic information can be found in the Supplementary Materials (Table S1). CCDC entries 1017003–1017008 contain the supplementary crystallographic data for this paper. These data can be obtained free of charge via http://www.ccdc.cam.ac.uk/conts/retrieving.html (accessed on 16 August 2021).

2.1. Synthesis of Neutral Zinc(II) Complexes

General Procedure

[Zn(LH$_2$)Cl$_2$] (**1**): A hot methanolic (20 mL) solution of **LH$_2$** (185 mg, 0.689 mmol) was added to a hot methanolic solution of zinc(II) chloride (110 mg, 0.807 mmol) in a 50-mL round bottom flask under nitrogen atmosphere. The above reaction mixture was allowed to reflux for 2 h, and the reaction progress was monitored through thin layer chromatography. During the reaction, an orange-red solid was precipitated. The solid that formed was filtered off, washed with cold methanol, and dried in vacuo. Single crystals suitable for X-ray diffraction analysis were grown from a mixture of an acetonitrile-water solution at room temperature. Yield (0.253 g, 90%), elemental analysis calcd (%) for $C_{14}H_{19}Cl_2N_6O_{1.5}Zn$ (**1**·$(H_2O)_{1.5}$): C 38.96, H 4.44, N 19.47; found: C 38.73, H 3.62, N 19.75. ^{1}H-NMR (400 MHz, D_2O): 2.36 (*s*, 6H, CH_3), 7.12 (*pseudo d*, 2H, J = 8.5 Hz, py-H4), 7.16 (*pseudo d*, 2H, J = 7 Hz, py-H2), 7. 92 (*pseudo dt*, 2H, J = 9 Hz, J = 1.5 Hz, PyH3), 8.36 (*pseudo d*, 2H, J = 5 Hz, py-H1); the NH signal could not be identified due to the fast H-D exchange in D_2O. ^{13}C-NMR (100 MHz, D_2O): 13.06 (CH_3), 111.82, 118.74, 142.13, 146.45 (pyridine carbons), 152.85 (imine carbon) ppm. (ESI): *m/z* (%): 331.6 $[LH(Zn)]^+$ (100), 369.3 $[LH_2(Zn)(H)Cl]^+$ (57.4). A similar procedure was used to prepare all the neutral zinc(II) complexes.

[Zn(LH$_2$)(OAc)$_2$] (**2**): Complex **2** was prepared analogously as complex **1** starting from 0.11 g of **LH$_2$**. Yield (0.103 g, 50%), elemental analysis calcd (%) for $C_{19}H_{28}N_6O_6Zn$ (**2**·MeOH·H_2O): C 45.47, H 5.62, N 16.75; found: C 45.81, H 4.58, N 16.80. ^{1}H-NMR (400 MHz, D_2O): 1.9 (6H, s, OAc), 2.35 (6H, s, CH_3), 7.10 (*pseudo d*, 2H, J = 9 Hz, py-H4), 7.16 (*pseudo d*, 2H, J = 6 Hz, py-H2), 7.92 (*pseudo dt*, 2H, J = 9 Hz, J = 3 Hz, pyH3), 8.36 (*pseudo d*, 2H, J = 6 Hz, py-H1); the NH signal could not be identified due to the fast H-D exchange in D_2O. ^{13}C-NMR (100 MHz, D_2O): 13.02 (CH_3), 23.46 (OAc) 111.62, 118.52, 141.97, 146.67 (pyridine carbons), 152.87 (imine carbon), 181.93 (acetyl carbon) ppm. (ESI): *m/z* (%): 331.1 $[LH(Zn)]^+$ (100), 599.1 $[(LH_2)(LH)Zn]^+$ (100).

[Zn(LH$_2$)(N$_3$)$_2$] (**3**): A 15-mL methanol solution of complex **1** (50 mg, 0.0124 mmol) and NaN_3 (16 mg, 0.0246 mmol) was mixed in 10 mL of water and stirred at room temperature overnight. The progress of the reaction was monitored by TLC. After the completion of the reaction, the reaction mass was filtered, and the corresponding filtrate was slowly evaporated at room temperature. The greenish yellow crystals of $[Zn(L)(N_3)_2]$ (**3**) were isolated (43 mg, 83% yield). Complex **3** was also prepared by the reaction of ligand (**LH$_2$**) with $ZnCl_2/NaN_3$ (1:2 ratio), which were mixed with 15 mL of methanol and 5 mL of water and heated to reflux for 6 hours. The greenish yellow crystals of complex **3** were isolated with 73% yield. Elemental analysis calcd (%) for $C_{14}H_{17.5}N_{12}O_{0.75}Zn$ (**3**·$(H_2O)_{0.75}$): C 38.99, H 4.09, N 38.98; found: C 38.39, H 3.60, N 39.35. IR (cm^{-1}): 2898 (w), 2051 (m), 1605 (m), 1475 (m), 1427 (m), 772 (m). ^{1}H-NMR (400 MHz, DMSO-D_6): 2.22 (6H, s, CH_3), 6.80 (*pseudo dt*, 2H, J = 6.6 Hz, J = 1.4 Hz, py-H2), 7.23 (*pseudo d*, 2H, J = 8.4 Hz, py-H4), 7.66 (*pseudo dt*, 2H, J = 8.6 Hz, J = 1.68 Hz, py-H3), 8.14 (*pseudo d*, 2H, J = 4 Hz, py-H1), 9.70 (*br*, 2H, NH); ^{13}C-NMR (100 MHz, DMSO, Me_4Si): 10.60 (CH_3), 106.8, 115.4, 137.9, 144.9, 147.5, 157.3 (pyridine carbons) ppm. (ESI): *m/z* (%): 331.1 $[LH(Zn)]^+$ (100), 599.1 $[(LH_2)(LH)Zn]^+$ (100). ***CAUTION****: Owing to their potentially explosive nature, reaction with azide salts and their complexes should be performed with extreme care.*

[Zn(LH$_2$)(OTf)$_2$] (**4**): 100 mg of **LH$_2$** and 135 mg of $Zn(OTf)_2$ were dissolved in 10 mL of acetonitrile. After 24 h, the precipitated solid was isolated by filtration and drying. Yield (0.168 g, 71%), elemental analysis calcd (%) for $C_{16}H_{16}F_6N_6O_6S_2Zn$ C 30.42, H 2.55, N 13.30; found: C 30.24, H 2.52, N 13.19. ^{1}H-NMR (400 MHz, D_2O): 2.32 (6H, s, CH_3), 7.10 (*pseudo d*, 2H, J = 8.56 Hz, py-H4), 7.14 (*pseudo t*, 2H, J = 7.12 Hz, J = 0.88 Hz, py-H2), 7.90 (*pseudo dt* 2H, J = 8.76 Hz, J = 1.44 Hz, py-H3), 8.33 (*pseudo d*, 2H, J = 4.8 Hz, py-H1); the NH signal could not be identified due to the fast H-D exchange in D_2O. ^{13}C-NMR (100 MHz, D_2O, Me_4Si): 12.50 (CH_3), 111.31, 118.24, 141.65, 145.94 (pyridine carbons), 152.37 (imine carbon) ppm. (ESI): *m/z* (%): 331.1 $[LH(Zn)]^+$ (100); 367.1 $[LH_2(Zn)(H_2O+OH)]^+$ (100), 481.0 $[L(Zn)OTf]^+$ (100).

2.2. Synthesis of Deprotonated Complexes

[$Zn_2(L_2)$] (**5**): Zinc(II) bis(trimethylsilyl)amide (0.144 g, 0.37 mmol) in dry THF (5 mL) was added to a solution of ligand (**LH_2**) (0.1 g, 0.37 mmol) in dry THF (5 mL). After being stirred for 24 h at room temperature, the red-pink colored solution was filtered and crystallization was allowed to occur. Pink colored crystals suitable for single-crystal X-ray crystallography were obtained by room temperature evaporation. Yield (0.098 g, 80%), elemental analysis calcd (%) for $C_{28}H_{28}N_{12}Zn_2$ (660.12): C 50.70, H 4.25, N 25.34; found: C 50.39, H 4.31, N 25.01. It was unfortunately not possible to obtain an NMR spectrum only containing **5** due to its highly hygroscopic nature.

[$Fe(LH)_2$]·H_2O (**6**): Ligand (**LH_2**) (0.025 g, 0.0925 mmol) and iron(II) bis (trimethylsilyl) amide (0.035 g, 0.0929 mmol) were dissolved in 4 mL of dry acetonitrile. The reaction changed their color into a brownish red, and the reaction was stirred for 24 h at RT. The reaction mixture was filtered, and the resulting brownish red suspension was washed with pentane (10 mL). Single crystals of **6** were obtained by slow evaporation of the solvent from a saturated solution in dry acetonitrile, yield 11 mg (19%, based on iron salt). No useful NMR data could be obtained. Elemental analysis calcd (%) for $C_{28}H_{41.6}FeN_{12}O_{5.8}$ (**6**·$(H_2O)_{5.8}$): C 48.39, H 6.03, N 24.19; found: C 47.51, H 5.43, N 25.07. (ESI): *m/z* (%): 323.2 $[LH(Fe)]^+$ (100), 590.4 $[(LH)_2Fe]^+$ (100).

3. Results and Discussions

3.1. Synthesis and Characterization

The neutral N4-tetradentate ligand **LH_2** was prepared according to a procedure described in the literature [41,42] by employing the condensation reaction of two equivalents of 2-hydrazinopyridine and one equivalent of 2,3-butanedione. The prepared ligand **LH_2** was characterized by NMR and ESI-MS. The subsequent reactions between **LH_2** and the metal salts are shown in Scheme 2.

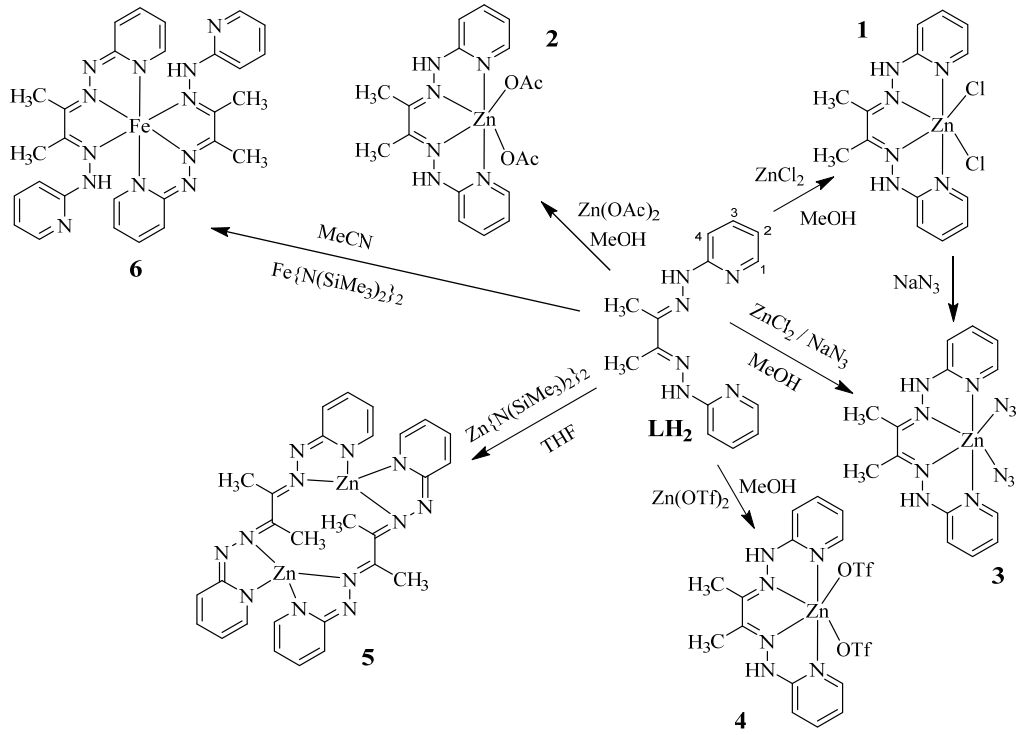

Scheme 2. Synthesis of zinc(II) **1**–**5** and iron(II) **6** complexes with neutral **LH_2**, mono-deprotonated **LH** and doubly deprotonated ligand **L**.

Complexes **1**, **2**, and **4** were synthesized from an equal molar ratio of ligand **LH_2** and ZnX_2 (X = Cl, OAc, and OTf) in the presence of methanol as a solvent. Complex **3** was

synthesized either from complex **1** or as complex **1** but in the presence of an additional two equivalents of sodium azide. In all of the reactions, coordination was immediate and followed by formation of a solid. The solid residue thus obtained was filtered and washed with cold methanol and diethyl ether. The yields of the complexes were relatively good, and the details are given in the experimental section. All the new complexes (**1**–**4**) were isolated as colorless to yellow, air stable solids, and are non-hygroscopic in nature. The synthesized complexes are highly soluble in water and DMSO, and partially soluble in chloroform. On the other hand, the Zn(II) complex **5** and the mono nuclear Fe(II) complex **6**, both with a deprotonated ligand, were synthesized in the glove box by treating an equal molar ratio of ligand and the corresponding silyl amide salts in either THF or acetonitrile as solvent (Scheme 2). The complexation processes were monitored by ^{1}H NMR spectroscopy. After the completion of the reaction, the solvent was evaporated, and the residue was washed with dry pentane.

The Zn-Zn dimer and iron(II) complexes are pink and brown colored solids, respectively, that are insoluble in apolar solvents but are highly soluble in chloroform and acetonitrile, respectively. The synthesized complexes **1**–**6** were characterized by X-ray and ESI-MS. Structural studies of complexes **1**–**4** showed that the ligand acts as a planar tetradentate chelate ligand coordinating through the imine and the pyridine nitrogen atoms, while in complex **5**, one bisdeprotonated ligand coordinates to two different zinc metal centers, and in complex **6**, each monodeprotonated ligand only coordinates with three nitrogen atoms to the iron.

*3.2. NMR Spectra of the Zinc Complexes **1**–**4***

Zinc complexes **1**–**4** were fully characterized, and their structures in solution were investigated in detail via NMR spectroscopy with the aim of understanding the coordination environment around the metal center. Zinc would be expected to elicit slight ^{1}H shift differences relative to the frequencies of the free ligands. The ^{1}H-NMR spectrum of the symmetrical complex **1** in D_2O shows five well-resolved signals: (i) four aromatic signals in the low-field region (between 6.5 and 8.2 ppm, detailed assignment in the experimental section); (ii) a sharp singlet around 2.30 ppm corresponding to the methyl protons of the ligand, which is slightly downfield shifted relative to the free ligand (2.22 ppm). Similar spectral patterns were also observed for the other neutral complexes **2**–**4** (see also the Supplementary Materials (Figures S1 and S2)). In the case of the zinc acetate complex **2**, an additional sharp singlet was observed to occur at 1.90 ppm.

3.3. Description of Crystal Structures

As part of the structural characterization, the molecular structures of complexes **1**–**6** were determined by single crystal x-ray analysis. Transparent crystals of complexes **1**–**4** suitable for X-ray diffraction analyses were obtained by the slow vapor diffusion of hexane into the saturated acetonitrile/dichloromethane solutions at ambient temperature [50]. On the contrary, crystals of the Zn-Zn dimer (**5**) and the iron(II) complex (**6**) were grown by slow evaporation of THF and acetonitrile, respectively, in the glove box. The ellipsoidal representations with atom numbering are shown in Figures 1–6, and selected bond lengths and angles are given in the corresponding figure captions. Crystal data and data collection details of complexes **1**–**6** are presented in Table S1. $Zn(LH_2)Cl_2$ (**1**) crystallized in the monoclinic space group P2/n. The molecular structure of complex **1** adopts an octahedral geometry, with the metal center being coordinated by the chelating N4 ligand (two pyridine and two imine nitrogen atoms) in the equatorial plane and by two axial chloride atoms. The two-fold axis of the space group bisects the C9-C9# bond. The equatorial coordination of the N4 ligand to the zinc center forces the two chloride ligands to be placed *trans* to each other with a bond angle of Cl(1)-Zn(1)-Cl(1)#1 that is 168.81(3)°. This is one of the few *trans* bond angles that is off 180° for ZnN_4Cl_2 complexes [51–53] (see the following references with examples of 180° Cl-Zn-Cl bond angles: [54,55]). Notably, 29 out of 40 of the ZnN_4Cl_2 complexes in the CSD database [56] actually have a *cis* arrangement of the

chlorides (see [57,58]). All of the bond distances and bond angles in the crystal structure are comparable with similar distances in other structurally characterized six-coordinate zinc(II) complex-containing terminal chlorides [59,60].

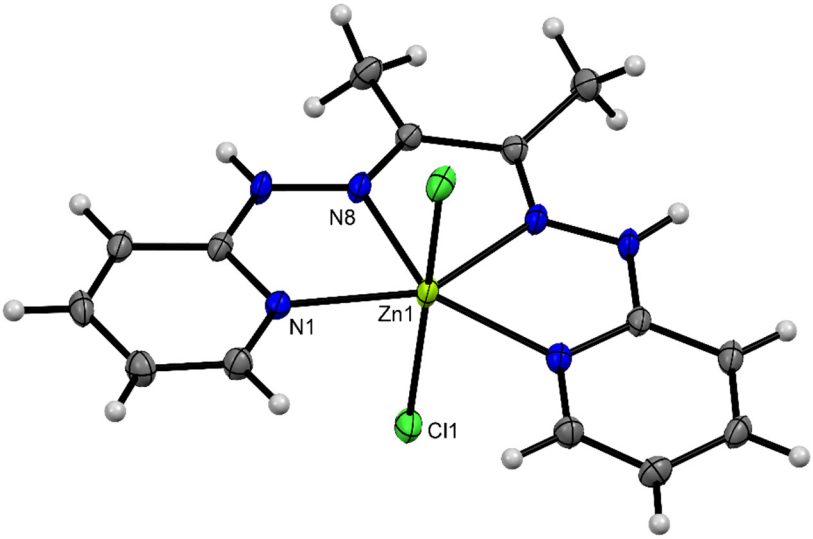

Figure 1. Ellipsoidal representation of $[Zn(LH_2)Cl_2]$ (**1**) showing 50% thermal ellipsoids. Selected bond lengths [Å] and angles [°]: Zn1-N1 = 2.1330(18), Zn1-N8 = 2.1352(18), Zn1-Cl1 = 2.4899(6), N(1)-Zn(1)-N(1)#1 = 137.81(10), Cl(1)-Zn(1)-Cl(1)#1 = 168.81(3).

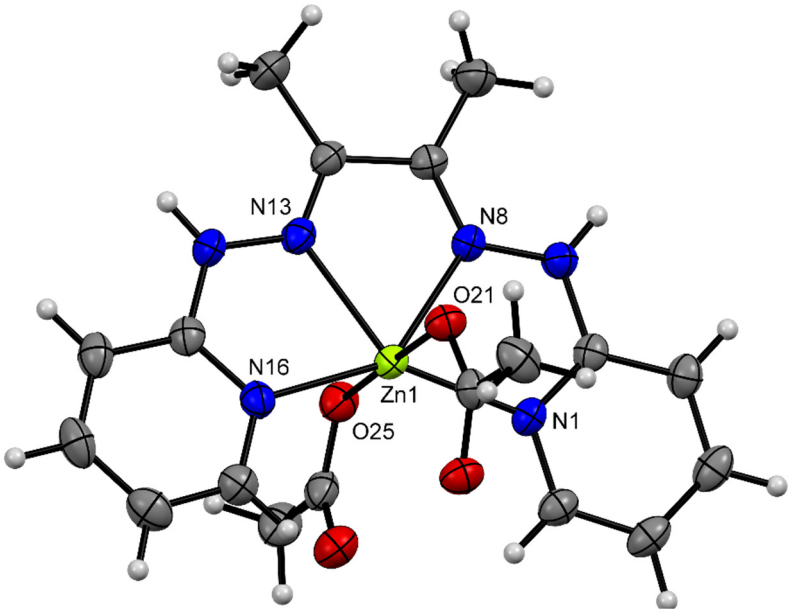

Figure 2. Ellipsoidal representation of $[Zn(LH_2)(OAc)_2]\cdot H_2O$ (**2**) showing 50% thermal ellipsoids (the water molecule was omitted for clarity). Selected bond lengths [Å] and angles [°]: Zn1-N1 = 2.176(2), Zn1-N8 = 2.190(2), Zn1-N13 = 2.205(2), Zn1-N16 = 2.177(2), Zn1-O21 = 2.063(2), Zn1-O25 = 2.091(2), N(1)-Zn(1)-N(16) = 143.66(9), O(21)-Zn(1)-O(25) = 178.71(9).

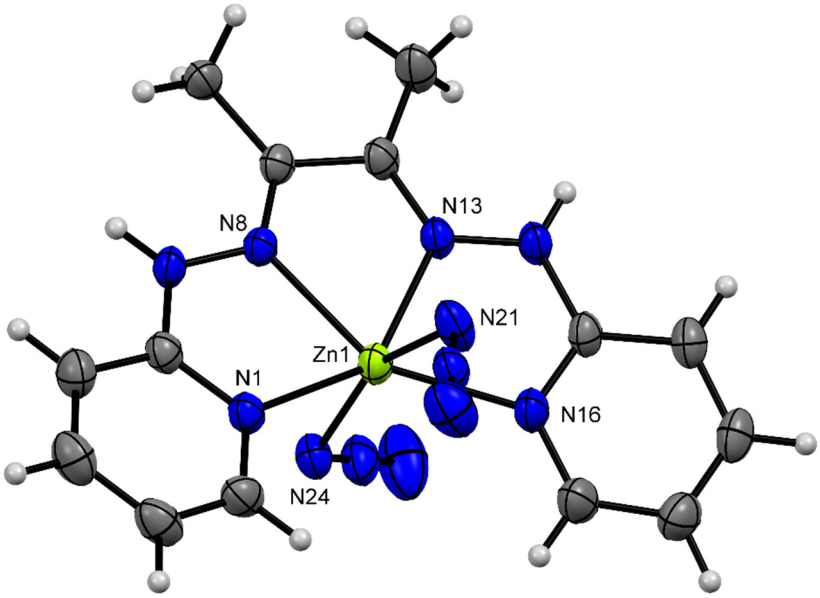

Figure 3. Ellipsoidal representation of $[Zn(LH_2)(N_3)_2]$ (**3**) showing 50% thermal ellipsoids. Selected bond lengths [Å] and angles [°]: Zn1-N1 = 2.219(2), Zn1-N8 = 2.163(2), Zn1-N13 = 2.175(2), Zn1-N16 = 2.284(2), Zn1-N21 = 2.090(2), Zn1-N24 = 2.100(2), N(1)-Zn(1)-N(16) = 144.01(8), N(21)-Zn(1)-N(24) = 158.44(10).

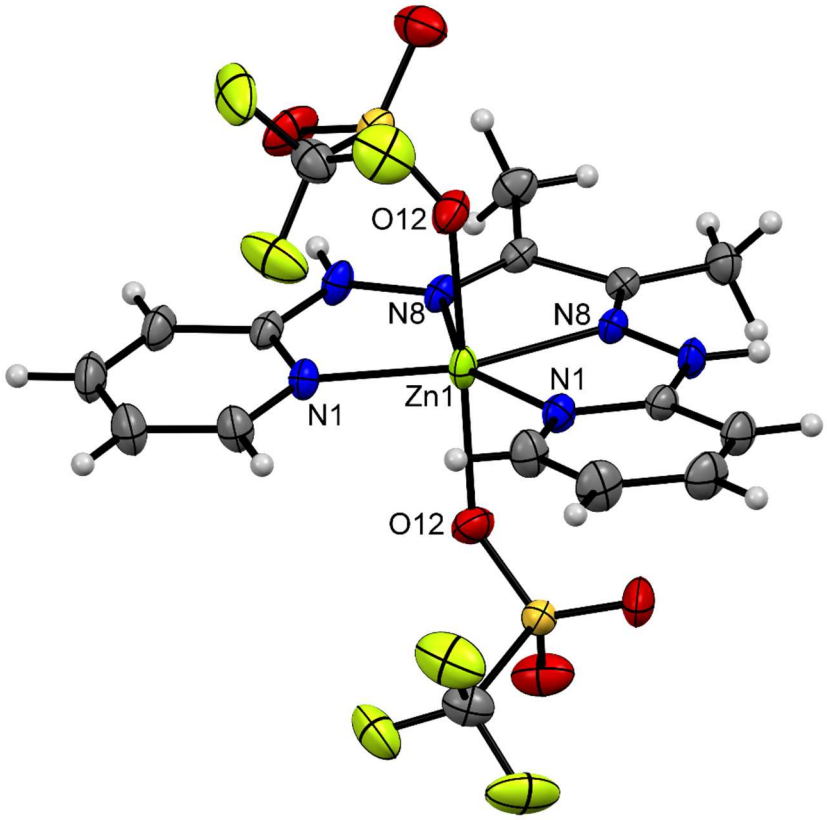

Figure 4. Ellipsoidal representation of $[Zn(LH_2)(OTf)_2]$ (**4**) showing 50% thermal ellipsoids. Selected bond lengths [Å] and angles [°]: Zn(1)-N(1) = 2.0445(15), Zn(1)-N(8) = 2.1052(16), Zn(1)-O(12) = 2.2535(14), N(1)-Zn(1)-N(1)#1 = 131.48(10), O(12)-Zn(1)-O(12)#1 = 178.26(8).

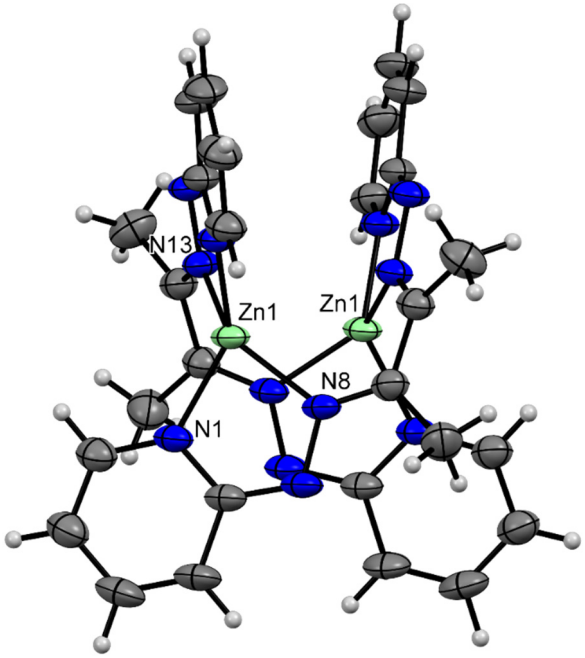

Figure 5. Ellipsoidal representation of $[Zn_2L_2]$ (**5**) showing 50% thermal ellipsoids. Selected bond lengths [Å] and angles [°]: Zn(1)-N(1) = 1.967(3), Zn(1)-N(8) = 2.018(3), Zn(1)···Zn(1)#1 = 3.0833(10), N(1)-Zn(1)-N(8) = 81.62(13), N(1)-Zn(1)-N(13)#1 = 115.51(13), N(13)#1-Zn(1)-N(8) = 137.79(12). #1: 0.5−x, y, 1−z.

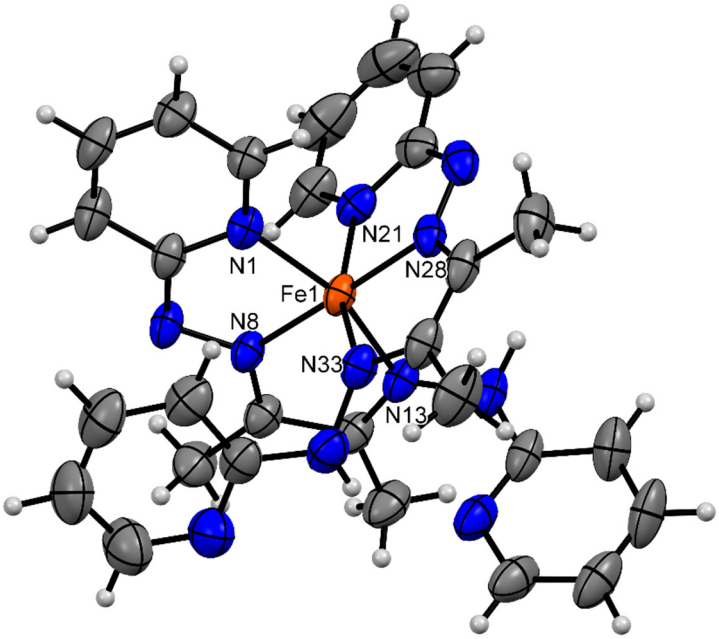

Figure 6. Ellipsoidal representation of $[Fe(LH)_2]\cdot H_2O$ (**6**) showing 50% thermal ellipsoids (a water molecule was omitted for clarity). Selected bond lengths [Å] and angles [°]: Fe(1)-N(1) = 1.954(2), Fe(1)-N(8) = 1.878(2), Fe(1)-N(13) = 1.959(2), Fe(1)-N(21) = 1.956(2), Fe(1)-N(28) = 1.867(2), Fe(1)-N(33) = 1.968(2), N(1)-Fe(1)-N(13) = 159.51(10), N(21)-Fe(1)-N(33) = 160.18(11).

The ligand LH_2 has an essentially planar ligand geometry in complexes **1**–**4**. The following corresponding O-Zn-O bond angles are quite similar for **2** (178.66(10)°) and **4** (178.26(8)°). On the other hand, the N-Zn-N angle in **3** is 158.44(10)°. The azide units are linear; they coordinate to the zinc metal with Zn-N-N angles of 116.49(15)° and 118.63(16)°, respectively. This bent-on coordination of inorganic azides to metal centers has been very

nicely explained by Dori et al. [61]. There has been only one previously reported $ZnN_4(N_3)_2$ complex with the two azides in *trans* position that have an N(azide)-Zn-N(azide) angle off 180° [62]. Again, all of the other reported $ZnN_4(N_3)_2$ complexes with the two azides in *trans* position have a N(azide)-Zn-N(azide) angle of exactly 180° (see, for example, [63]).

Furthermore, the pink-red and dark brown-colored crystals corresponding to **5** and **6** were isolated by the reaction of the ligand with $[Zn\{N(SiMe_3)_2\}_2]$ and $[Fe\{N(SiMe_3)_2\}_2]$, respectively, in the presence of dry THF solvent. The crystals (**5**, **6**) that were formed are thermally stable and can be crystallized after workup from pentane and evaporation at room temperature. Complex **5** crystallizes in the monoclinic space group I2/a (Figure 5), and the representation of the asymmetric unit of complex **5** is given in the Supplementary Materials (Figure S3). Examination of the solid-state structure reveals it to be a neutral complex in which each zinc atom in this molecule is four-fold coordinated and is surrounded by two imine and two pyridine nitrogen donors. The double deprotonation from either side of NH generates the dearomatized Zn-Zn dimer, and the dearomatized structure is clearly indicated by the considerably shorter C2−N7 bond (1.339(5)–1.350(6) Å) compared to the analogue bond distances in the neutral zinc(II) complexes (**1**–**4**) (1.377(3)–1.390(4) Å) (see Figure 7). The distance between the Zn· · · Zn centers (3.0857(10) Å) is a very comparable range to that found in other dimeric zinc(II) complexes with tetrahedral arrangements [64,65].

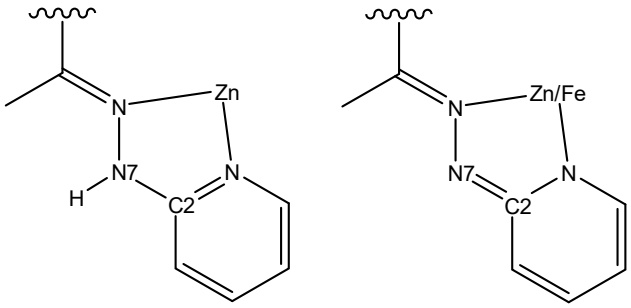

Figure 7. Comparison of the bonding in complexes **1**–**4** (**left**) and **5**/**6** (**right**).

In the iron(II) crystal structure, the ligand underwent NH deprotonation on one side followed by the iron coordination with three nitrogen atoms (two imine nitrogen and one pyridine nitrogen atom). The coordination sphere of the iron center is completed with a second equally monodeprotonated ligand (Figure 7).

In complex **1**, the one crystallographically independent N-H forms a weak hydrogen bond to a neighboring chloride anion: N7-H7 Cl1(1−x,−y,2−z), 3.232(2) Å. In complex **2**, the two N-H moieties form hydrogen bonds to a neighboring acetate and water molecule, respectively: N7-H7 O23(x,−1/2+y,1/2−z), 2.771(3) Å and N14-H14 O31(1−x,−y,1−z), 2.814(4) Å. In complex **3**, the two N-H moieties form hydrogen bonds to neighboring azide moieties: N7-H7 N24(1−x,2−y,2−z), 2.974(3) Å and N14-H14 N21, 2.906(3) Å. In complex **4**, the one crystallographically independent N-H moiety forms a hydrogen bond to a neighboring triflate anion: N7-H7 O13(−1/2+x,1/2−y,−1/2+z), 2.844(2) Å. In complex **6**, the one N-H moiety forms a hydrogen bond to a water molecule: N14-H14 O41, 2.837(5) Å. This water molecule in turn forms two hydrogen bonds to two neighboring deprotonated nitrogen atoms (N27 and N28): O41-H41A N27(1−x,−y,1−z), 2.829(4) and O41-H41B N27, 2.866(4) Å.

4. Conclusions

In conclusion, we have reported a new series of neutral, mono, and doubly deprotonated zinc(II) and iron(II) complexes containing N4 ligand $\mathbf{LH_n}$ (n: 0–2). The synthesized complexes (**1**–**6**) have been carefully studied by extensive spectroscopic and structural characterization. Single crystal X-ray diffraction method revealed that an N4 neutral ligand was coordinated to iron(II) and zinc(II) via two imine nitrogen atoms and pyridine nitrogen

and demonstrated the presence of a typical four- and six-coordinate geometry around the metal center. Interestingly, complex **5** represents an unusual four coordination of two zinc centers along with two molecules of doubly deprotonated ligand. On the other hand, complex **6** shows a distorted octahedral geometry around iron(II) with two molecules of mono-deprotonated ligand.

Supplementary Materials: The following data are available online at https://www.mdpi.com/article/10.3390/cryst11080982/s1, Table S1: Crystallographic Information. Figure S1: ^{1}H-NMR spectrum of **3**. Figure S2: ^{1}H-NMR spectrum of **4**. Figure S3: Crystal structure of complex **5** (Asymmetric unit).

Author Contributions: Conceptualization: D.P. and B.S.; investigation: D.P., T.F. and B.S.; formal analysis: D.P., T.F. and B.S.; writing—original draft preparation: D.P.; writing—review and editing: B.S.; visualization: D.P. and B.S.; supervision: B.S.; project administration: B.S.; funding acquisition: D.P. and B.S. All authors have read and agreed to the published version of the manuscript.

Funding: This research was funded by the Swiss Government Excellence Scholarships for Foreign Scholars.

Acknowledgments: We thank the Department of Chemistry of the University of Zurich and the whole Alberto group for their valuable discussions. We further thank H. Spring for the elemental analyses and L. Schneider for the IR analysis.

Conflicts of Interest: The authors declare no conflict of interest. The funders had no role in the design of the study; in the collection, analyses, or interpretation of data; in the writing of the manuscript, or in the decision to publish the results.

References

1. Lippard, S.J.; Berg, J.M. *Principles of Bioinorganic Chemistry*; University Science Books: Melville, NY, USA, 1994; p. 411.
2. Haas, K.L.; Franz, K.J. Application of Metal Coordination Chemistry To Explore and Manipulate Cell Biology. *Chem. Rev.* **2009**, *109*, 4921–4960. [CrossRef]
3. Kaim, W.; Schwederski, B.; Klein, A. *Bioinorganic Chemistry: Inorganic Elements in the Chemistry of Life: An Introduction and Guide*, 2nd ed.; Wiley: Hoboken, NJ, USA, 2013; p. 426.
4. Liu, J.; Chakraborty, S.; Hosseinzadeh, P.; Yu, Y.; Tian, S.; Petrik, I.; Bhagi, A.; Lu, Y. Metalloproteins Containing Cytochrome, Iron–Sulfur, or Copper Redox Centers. *Chem. Rev.* **2014**, *114*, 4366–4469. [CrossRef]
5. Sekar, N.; Ramasamy, R.P. Recent advances in photosynthetic energy conversion. *J. Photochem. Photobiol. C* **2015**, *22*, 19–33. [CrossRef]
6. Proppe, A.H.; Li, Y.C.; Aspuru-Guzik, A.; Berlinguette, C.P.; Chang, C.J.; Cogdell, R.; Doyle, A.G.; Flick, J.; Gabor, N.M.; van Grondelle, R.; et al. Bioinspiration in light harvesting and catalysis. *Nat. Rev. Mat.* **2020**, *5*, 828–846. [CrossRef]
7. Kaminskaia, N.V.; Spingler, B.; Lippard, S.J. Hydrolysis of beta-Lactam Antibiotics Catalyzed by Dinuclear Zinc(II) Complexes—Functional Mimics of Metallo-beta-lactamases. *J. Am. Chem. Soc.* **2000**, *122*, 6411–6422. [CrossRef]
8. Kaminskaia, N.V.; Spingler, B.; Lippard, S.J. Intermediate in beta-lactam hydrolysis catalyzed by a dinuclear zinc(II) complex: Relevance to the mechanism of metallo-beta-lactamase. *J. Am. Chem. Soc.* **2001**, *123*, 6555–6563. [CrossRef] [PubMed]
9. Malina, J.; Hannon, M.J.; Brabec, V. Recognition of DNA bulges by dinuclear iron(II) metallosupramolecular helicates. *FEBS J.* **2014**, *281*, 987–997. [CrossRef] [PubMed]
10. Medina-Molner, A.; Rohner, M.; Pandiarajan, D.; Spingler, B. Mono- and dinuclear metal complexes containing the 1,5,9-triazacyclododecane ([12]aneN$_3$) unit and their interaction with DNA. *Dalton Trans.* **2015**, *44*, 3664–3672. [CrossRef]
11. Mahapatra, D.K.; Bharti, S.K.; Asati, V.; Singh, S.K. Perspectives of medicinally privileged chalcone based metal coordination compounds for biomedical applications. *Eur. J. Med. Chem.* **2019**, *174*, 142–158. [CrossRef] [PubMed]
12. Kumar, N.; Roopa; Bhalla, V.; Kumar, M. Beyond zinc coordination: Bioimaging applications of Zn(II)-complexes. *Coord. Chem. Rev.* **2021**, *427*, 213550. [CrossRef]
13. Schiff, H. Eine neue Reihe organischer Basen. *Justus Liebigs Ann. Chem.* **1864**, *131*, 118–119. [CrossRef]
14. Bermejo, E.; Castineiras, A.; Garcia, I.; West, D.X. Spectral and structural studies of mercury(II) complexes of 2-pyridineformamide N(4)-dimethylthiosemicarbazone. *Polyhedron* **2003**, *22*, 1147–1154. [CrossRef]
15. Abou Melha, K.S. In-vitro antibacterial, antifungal activity of some transition metal complexes of thiosemicarbazone Schiff base (HL) derived from N^4-(7′-chloroquinolin-4′-ylamino) thiosemicarbazide. *J. Enzyme Inhib. Med. Chem.* **2008**, *23*, 493–503. [CrossRef] [PubMed]
16. Zoubi, W.A. Biological Activities of Schiff Bases and Their Complexes: A Review of Recent Works. *Int. J. Org. Chem.* **2013**, *3*, 73–95. [CrossRef]

17. Abu-Dief, A.M.; Mohamed, I.M.A. A review on versatile applications of transition metal complexes incorporating Schiff bases. *Beni-Suef Univ. J. Bas. Appl. Sci.* **2015**, *4*, 119–133. [CrossRef] [PubMed]
18. Dalia, S.A.; Afsan, F.; Hossain, M.S.; Khan, M.N.; Zakaria, C.; Zahan, M.K.E.; Ali, M. A short review on chemistry of schiff base metal complexes and their catalytic application. *Int. J. Chem. Stud.* **2018**, *6*, 2859–2866.
19. More, M.S.; Joshi, P.G.; Mishra, Y.K.; Khanna, P.K. Metal complexes driven from Schiff bases and semicarbazones for biomedical and allied applications: A review. *Mater. Today Chem.* **2019**, *14*, 100195. [CrossRef]
20. Ziessel, R. Schiff-based bipyridine ligands. Unusual coordination features and mesomorphic behaviour. *Coord. Chem. Rev.* **2001**, *216*, 195–223. [CrossRef]
21. Cozzi, P.G. Metal-Salen Schiff base complexes in catalysis: Practical aspects. *Chem. Soc. Rev.* **2004**, *33*, 410–421. [CrossRef] [PubMed]
22. Gupta, K.C.; Sutar, A.K. Catalytic activities of Schiff base transition metal complexes. *Coord. Chem. Rev.* **2008**, *252*, 1420–1450. [CrossRef]
23. Costes, J.-P.; Shova, S.; Wernsdorfer, W. Tetranuclear $[Cu\text{-}Ln]_2$ single molecule magnets: Synthesis, structural and magnetic studies. *Dalton Trans.* **2008**, 1843–1849. [CrossRef] [PubMed]
24. Gupta, K.C.; Kumar Sutar, A.; Lin, C.-C. Polymer-supported Schiff base complexes in oxidation reactions. *Coord. Chem. Rev.* **2009**, *253*, 1926–1946. [CrossRef]
25. Orio, M.; Jarjayes, O.; Kanso, H.; Philouze, C.; Neese, F.; Thomas, F. X-Ray Structures of Copper(II) and Nickel(II) Radical Salen Complexes: The Preference of Galactose Oxidase for Copper(II). *Angew. Chem. Int. Ed.* **2010**, *49*, 4989–4992. [CrossRef]
26. Adão, P.; Kuznetsov, M.L.; Barroso, S.; Martins, A.M.; Avecilla, F.; Pessoa, J.C. Amino Alcohol-Derived Reduced Schiff Base $V^{IV}O$ and V^{V} Compounds as Catalysts for Asymmetric Sulfoxidation of Thioanisole with Hydrogen Peroxide. *Inorg. Chem.* **2012**, *51*, 11430–11449. [CrossRef] [PubMed]
27. Gong, D.; Wang, B.; Jia, X.; Zhang, X. The enhanced catalytic performance of cobalt catalysts towards butadiene polymerization by introducing a labile donor in a salen ligand. *Dalton Trans.* **2014**, *43*, 4169–4178. [CrossRef]
28. Oberholzer, M.; Probst, B.; Bernasconi, D.; Spingler, B.; Alberto, R. Photosensitizing Properties of Alkynylrhenium(I) Complexes $[Re(\text{-}C{\equiv}C\text{-}R)(CO)_3(N{\cap}N)]$ ($N{\cap}N$ = 2,2′-bipy, phen) for H_2 Production. *Eur. J. Inorg. Chem.* **2014**, 3002–3009. [CrossRef]
29. Das, P.; Linert, W. Schiff base-derived homogeneous and heterogeneous palladium catalysts for the Suzuki–Miyaura reaction. *Coord. Chem. Rev.* **2016**, *311*, 1–23. [CrossRef]
30. Beigi, Z.; Kianfar, A.H.; Farrokhpour, H.; Roushani, M.; Azarian, M.H.; Mahmood, W.A.K. Synthesis, characterization and spectroscopic studies of nickel (II) complexes with some tridentate ONN donor Schiff bases and their electrocatalytic application for oxidation of methanol. *J. Mol. Liq.* **2018**, *249*, 117–125. [CrossRef]
31. Liu, X.; Manzur, C.; Novoa, N.; Celedón, S.; Carrillo, D.; Hamon, J.-R. Multidentate unsymmetrically-substituted Schiff bases and their metal complexes: Synthesis, functional materials properties, and applications to catalysis. *Coord. Chem. Rev.* **2018**, *357*, 144–172. [CrossRef]
32. Mosberger, M.; Probst, B.; Spingler, B.; Alberto, R. Influence of Hetero-Biaryl Ligands on the Photo-Electrochemical Properties of $[Re^{I}NCS(N{\cap}N)(CO)_3]$-Type Photosensitizers. *Eur. J. Inorg. Chem.* **2019**, *2019*, 3518–3525. [CrossRef]
33. Wesley Jeevadason, A.; Kalidasa Murugavel, K.; Neelakantan, M.A. Review on Schiff bases and their metal complexes as organic photovoltaic materials. *Renew. Sustain. Energy Rev.* **2014**, *36*, 220–227. [CrossRef]
34. Ganguly, A.; Basu, S.; Banerjee, K.; Chakraborty, P.; Sarkar, A.; Chatterjee, M.; Chaudhuri, S.K. Redox active copper chelate overcomes multidrug resistance in T-lymphoblastic leukemia cell by triggering apoptosis. *Mol. BioSyst.* **2011**, *7*, 1701–1712. [CrossRef]
35. Ghosh, R.D.; Chakraborty, P.; Banerjee, K.; Adhikary, A.; Sarkar, A.; Chatterjee, M.; Das, T.; Choudhuri, S.K. The molecular interaction of a copper chelate with human P-glycoprotein. *Mol. Cell. Biochem.* **2012**, *364*, 309–320. [CrossRef] [PubMed]
36. Ganguly, A.; Chakraborty, P.; Banerjee, K.; Choudhuri, S.K. The role of a Schiff base scaffold, N-(2-hydroxy acetophenone) glycinate-in overcoming multidrug resistance in cancer. *Eur. J. Pharm. Sci.* **2014**, *51*, 96–109. [CrossRef] [PubMed]
37. Geldard, J.F.; Lions, F. Tridentate Chelate Compounds. III. *Inorg. Chem.* **1963**, *2*, 270–282. [CrossRef]
38. Chiswell, B.; Lions, F. Quadridentate Chelate Compounds. 4. Metal Complexes from Butane-2,3-Dione Bis(2′-Pyridylhydrazone). *Inorg. Chem.* **1964**, *3*, 490–493. [CrossRef]
39. Bailey, N.A.; James, T.A.; McCleverty, J.A.; McKenzie, E.D.; Moore, R.D.; Worthington, J.M. Novel Class of Dimeric Nickel(II) Compounds with Quadridentate Nitrogen Ligands—Crystal-Structure of $[Ni_2(C_{16}H_{16}N_6)_2]$. *J. Chem. Soc. Chem. Commun.* **1972**, *11*, 681–682. [CrossRef]
40. Bailey, N.A.; McKenzie, E.D.; Worthington, J.M. Structure and Redox Properties of Some Planar $[M^{11}N_4]$ Chelate Compounds of Cobalt and Nickel. 3. Crystal and Molecular-Structure of Bis[Cyclohexane-1,2-Bis-2′-Pyridyl-Hydrazonato]-Dinickel(II), 2-Benzene. *Inorg. Chim. Acta* **1980**, *43*, 145–153. [CrossRef]
41. Guhathakurta, B.; Pradhan, A.B.; Das, S.; Bandyopadhyay, N.; Lu, L.; Zhu, M.; Naskar, J.P. Spectroscopic and molecular docking studies on the interaction of human serum albumin with copper(II) complexes. *Spectrochim. Acta A* **2017**, *173*, 740–748. [CrossRef]
42. Guhathakurta, B.; Biswas, C.; Naskar, J.P.; Lu, L.P.; Zhu, M.L. Synthesis and Crystal Structure of $[Cu(BDBPH)(ClO_4)_2]$ (BDBPH = Butane-2,3-dione bis(2′-pyridylhydrazone). *J. Chem. Crystallogr.* **2011**, *41*, 1694–1699. [CrossRef]
43. Ohki, Y.; Ohta, S.; Tatsumi, K.; Davis, L.M.; Girolami, G.S.; Royer, A.M.; Rauchfuss, T.B. Monomeric iron(II) complexes having two sterically hindered arylthiolates. *Inorg. Synth.* **2010**, *35*, 137–143.

44. Darensbourg, D.J.; Holtcamp, M.W.; Struck, G.E.; Zimmer, M.S.; Niezgoda, S.A.; Rainey, P.; Robertson, J.B.; Draper, J.D.; Reibenspies, J.H. Catalytic activity of a series of Zn(II) phenoxides for the copolymerization of epoxides and carbon dioxide. *J. Am. Chem. Soc.* **1999**, *121*, 107–116. [CrossRef]
45. Agilent Technologies. *CrysAlisPro Software System, 171.36*; Agilent Technologies: Oxford, UK, 2013.
46. Altomare, A.; Burla, M.C.; Camalli, M.; Cascarano, G.L.; Giacovazzo, C.; Guagliardi, A.; Moliterni, A.G.G.; Polidori, G.; Spagna, R. SIR97: A new tool for crystal structure determination and refinement. *J. Appl. Cryst.* **1999**, *32*, 115–119. [CrossRef]
47. Sheldrick, G.M. Crystal structure refinement with *SHELXL*. *Acta Cryst.* **2015**, *C71*, 3–8. [CrossRef]
48. Spek, A.L. Single-crystal structure validation with the program PLATON. *J. Appl. Cryst.* **2003**, *36*, 7–13. [CrossRef]
49. Macrae, C.F.; Sovago, L.; Cottrell, S.J.; Galek, P.T.A.; McCabe, P.; Pidcock, E.; Platings, M.; Shields, G.P.; Stevens, J.S.; Towler, M.; et al. *Mercury 4.0*: From visualization to analysis, design and prediction. *J. Appl. Cryst.* **2020**, *53*, 226–235. [CrossRef]
50. Spingler, B.; Schnidrig, S.; Todorova, T.; Wild, F. Some thoughts about the single crystal growth of small molecules. *CrystEngComm* **2012**, *14*, 751–757. [CrossRef]
51. Alcock, N.W.; Berry, A.; Moore, P. Structure of a complex of 1,4,8,11-tetraazacyclotetradecane (cyclam) with zinc(II) chloride. *Acta Cryst.* **1992**, *C48*, 16–19. [CrossRef]
52. Liang, X.-Q.; Xiao, H.-P.; Liu, B.-L.; Li, Y.-Z.; Zuo, J.-L.; You, X.-Z. Syntheses, structures and luminescent properties of four d10-metal coordination polymers based on the 2,4,5-tri(4-pyridyl)-imidazole ligand. *Polyhedron* **2008**, *27*, 2494–2500. [CrossRef]
53. Wen, Y.; Sheng, T.; Hu, S.; Wang, Y.; Tan, C.; Ma, X.; Xue, Z.; Wang, Y.; Wu, X. Effect of anions on the self-assembly of Zn(II) with a hydrogenated Schiff base ligand: Structural diversity and photoluminescent properties. *CrystEngComm* **2013**, *15*, 2714–2721. [CrossRef]
54. Park, S.; Lee, J.K.; Lee, H.; Nayab, S.; Shin, J.W. Zinc (II), palladium (II) and cadmium (II) complexes containing 4-methoxy-N-(pyridin-2-ylmethylene) aniline derivatives: Synthesis, characterization and methyl methacrylate polymerization. *Appl. Organomet. Chem.* **2019**, *33*, e4797. [CrossRef]
55. Conradie, J.; Conradie, M.M.; Tawfiq, K.M.; Al-Jeboori, M.J.; Coles, S.J.; Wilson, C.; Potgieter, J.H. Novel dichloro(bis{2-[1-(4-methylphenyl)-1H-1,2,3-triazol-4-yl-κN3]pyridine-κN})metal(II) coordination compounds of seven transition metals (Mn, Fe, Co, Ni, Cu, Zn and Cd). *Polyhedron* **2018**, *151*, 243–254. [CrossRef]
56. Taylor, R.; Wood, P.A. A Million Crystal Structures: The Whole Is Greater than the Sum of Its Parts. *Chem. Rev.* **2019**, *119*, 9427–9477. [CrossRef]
57. Sakaguchi, Y.; Call, A.; Cibian, M.; Yamauchi, K.; Sakai, K. An earth-abundant system for light-driven CO_2 reduction to CO using a pyridinophane iron catalyst. *Chem. Commun.* **2019**, *55*, 8552–8555. [CrossRef] [PubMed]
58. Saghatforoush, L.; Moeini, K.; Golsanamlou, V.; Amani, V.; Bakhtiari, A.; Mardani, Z. Structural, spectral and theoretical study of the coordination of 3,6-bis(2-pyridyl)tetrazine ligand with zinc(II) and mercury(II). *Inorg. Chim. Acta* **2018**, *483*, 392–401. [CrossRef]
59. Neels, A.; Stoeckli-Evans, H. Trinuclear zinc(II) complexes and polymeric cadmium(II) complexes with the ligand 2,5-bis(2-pyridyl)pyrazine: Synthesis, spectral analysis, and single-crystal and powder X-ray analyses. *Inorg. Chem.* **1999**, *38*, 6164–6170. [CrossRef]
60. Yamamoto, Y.; Suzuki, T.; Kaizaki, S. Crystal structures, magnetic and spectroscopic properties of manganese(II), cobalt(II), nickel(II) and zinc(II) dichloro complexes bearing two 2-pyridyl-substituted imino nitroxides. *J. Chem. Soc. Dalton Trans.* **2001**, 1566–1572. [CrossRef]
61. Dori, Z.; Ziolo, R.F. Chemistry of coordinated azides. *Chem. Rev.* **1973**, *73*, 247–254. [CrossRef]
62. Ray, S.; Konar, S.; Jana, A.; Jana, S.; Patra, A.; Chatterjee, S.; Golen, J.A.; Rheingold, A.L.; Mandal, S.S.; Kar, S.K. Three new pseudohalide bridged dinuclear Zn(II), Cd(II) complexes of pyrimidine derived Schiff base ligands: Synthesis, crystal structures and fluorescence studies. *Polyhedron* **2012**, *33*, 82–89. [CrossRef]
63. Sunkari, S.S.; Kharediya, B.; Saha, S.; Elrez, B.; Sutter, J.-P. Chain of dimers to assembly of trimers: Temperature and ligand influenced formation of novel supramolecular assemblies of Cu(II) with isomeric (aminomethyl) pyridines and azide. *New J. Chem.* **2014**, *38*, 3529–3539. [CrossRef]
64. Chaudhuri, P.; Stockheim, C.; Wieghardt, K.; Deck, W.; Gregorzik, R.; Vahrenkamp, H.; Nuber, B.; Weiss, J. Mononuclear and Dinuclear Zinc(II) Complexes of Biological Relevance—Crystal-Structures of $[L_2Zn](PF_6)_2$, $[L'Zn(O_2CPh)_2(H_2O)]$, $[L'_2Zn_2(\mu\text{-}OH)_2](ClO_4)_2$, and $[L'_2Zn_2(\mu\text{-}OH)(\mu\text{-}CH_3CO_2)_2](ClO_4)\cdot H_2O$ (L = 1,4,7-Triazacyclononane, L' = 1,4,7-Trimethyl-1,4,7-Triazacyclononane). *Inorg. Chem.* **1992**, *31*, 1451–1457. [CrossRef]
65. González, D.M.; Cisterna, J.; Brito, I.; Roisnel, T.; Hamon, J.-R.; Manzur, C. Binuclear Schiff-base zinc(II) complexes: Synthesis, crystal structures and reactivity toward ring opening polymerization of rac-lactide. *Polyhedron* **2019**, *162*, 91–99. [CrossRef]

Supplementary Materials

An N4-tetradentate hydrazone ligand that binds in a neutral, mono- and bisdeprotonated form to iron(II) and zinc(II) metal ions

Devaraj Pandiarajan, Thomas Fox and Bernhard Spingler*

University of Zürich, Department of Chemistry, Winterthurerstr. 190, CH-8057 Zürich, Switzerland.

Fax: +41 44 635 68 02; E-mail: spingler@chem.uzh.ch.

Contents **Pages**

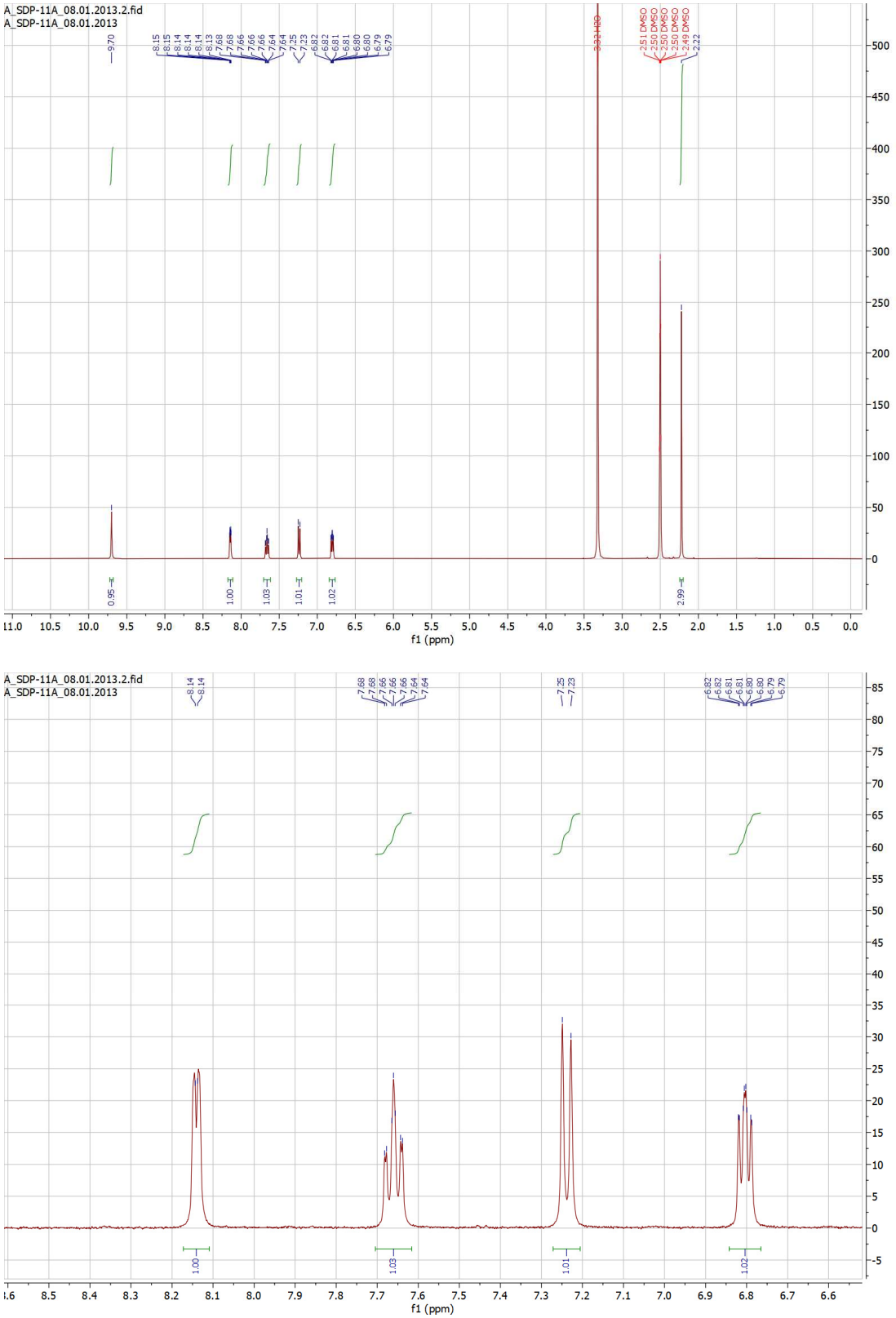

Figure S1. ^{1}H-NMR spectrum of complex **3** in $D_3CS(O)CD_3$ including enlargement of aromatic region.

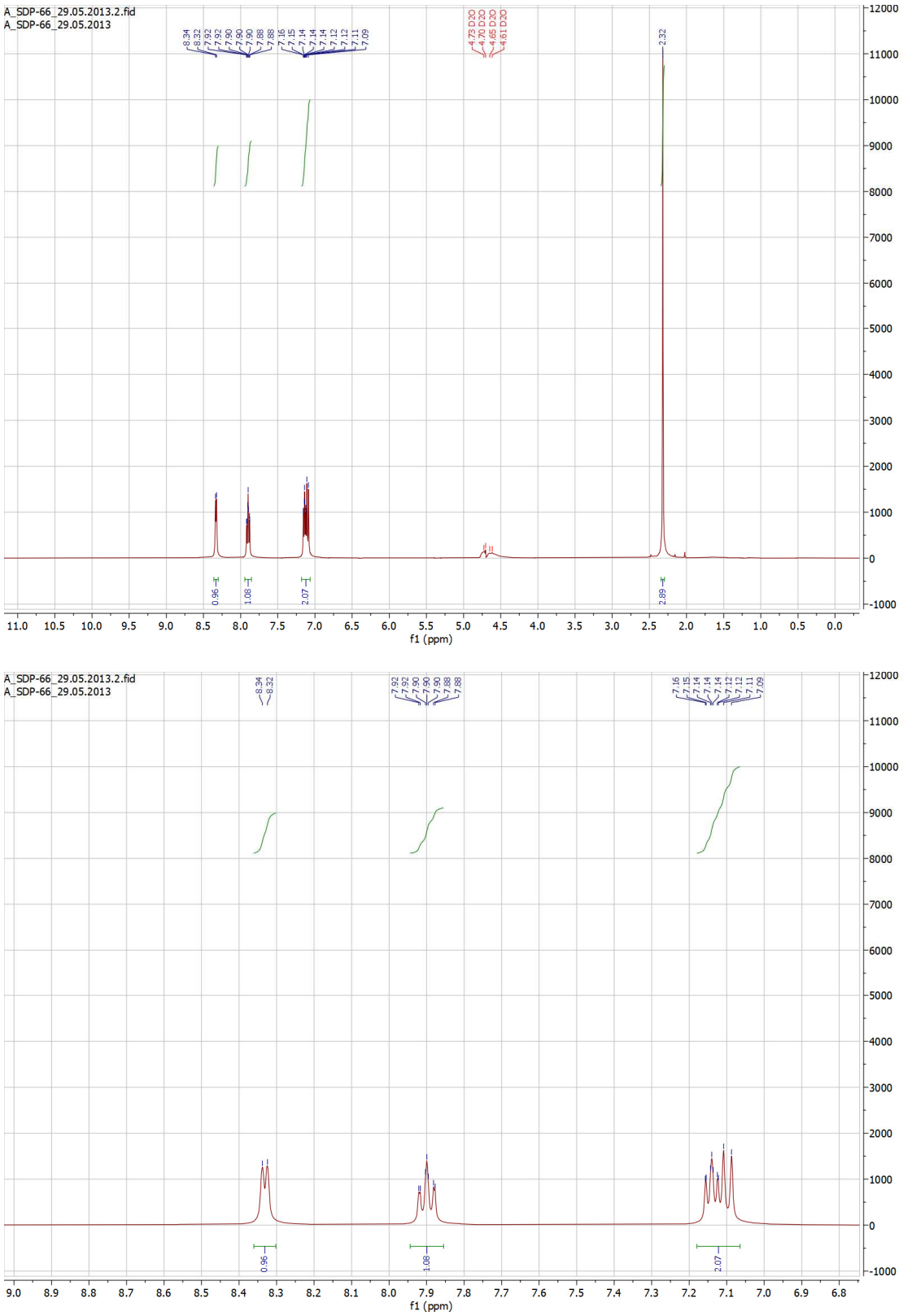

Figure S2. ^{1}H-NMR spectrum of complex **4** in D_2O including enlargement of aromatic region.

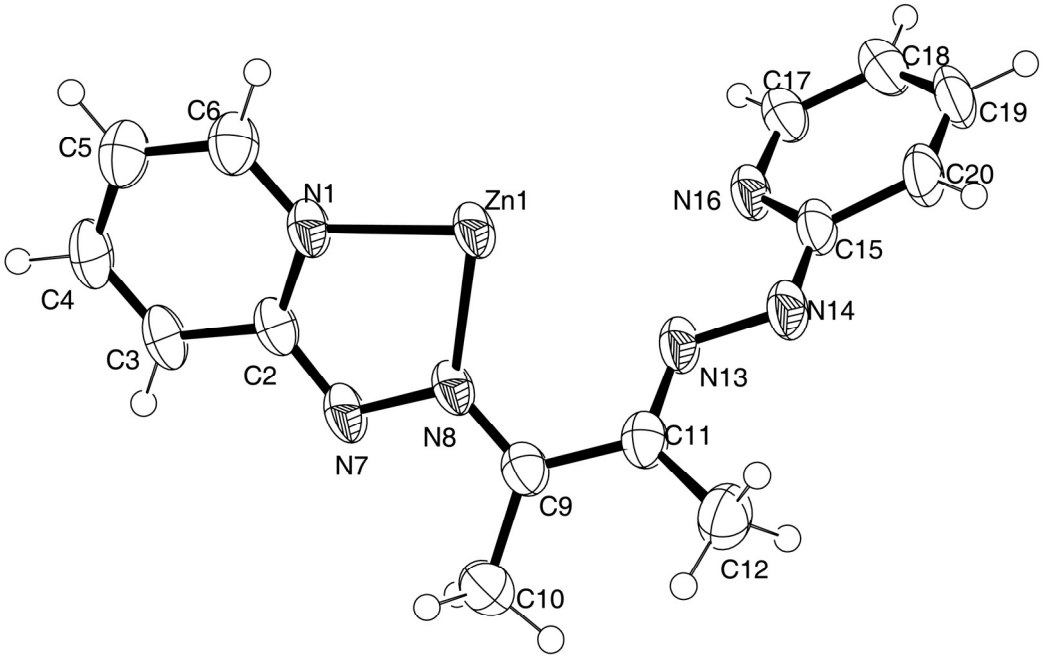

Figure S3. ORTEP representation of an asymmetric unit of the Zn-Zn dimer (**5**)

Table S1. Crystal data and structure refinement parameters for complexes **1**-**6**

Compounds	$[Zn(LH_2)Cl_2]$ (**1**)	$[Zn(LH_2)(OAc)_2]\cdot H_2O$ (**2**)	$[Zn(LH_2)(N_3)_2]$ (**3**)
Empirical formula	$C_{14}H_{16}Cl_2N_6Zn$	$C_{18}H_{24}N_6O_5Zn$	$C_{14}H_{16}N_{12}Zn$
Formula weight	404.60	469.80	417.76
Wavelength [Å]	0.71073	1.54184	1.54184
Crystal system	Monoclinic	Monoclinic	Triclinic
Space group	P 1 2/n 1	P 1 21/c 1	P-1
a [Å]	8.4935(5)	8.57160(14)	8.0537(2)
b [Å]	9.7578(6)	14.6873(2)	9.5480(3)
c [Å]	9.8536(6)	16.3014(2)	11.6897(3)
α [°]	90	90	81.461(2)
β [°]	100.795(6)	91.1754(13)	88.337(2)
γ [°]	90	90	77.855(3)
Volume [$Å^3$]	802.19(9)	2051.81(5)	869.04(4)
Z	2	4	2
Density (calculated) [Mg/m^3]	1.675	1.521	1.596
Absorption coefficient [mm^{-1}]	1.871	2.043	2.217
F(000)	412	976	428
Crystal size [mm^3]	0.22 x 0.17 x 0.04	0.12 x 0.1 x 0.06	0.16 x 0.05 x 0.04
Crystal description	light yellow plate	colorless prism	yellow needle
Theta range for data collection [°]	2.964 to 32.808	4.052 to 74.290	3.824 to 74.452
Index ranges	-8<=h<=12, -13<=k<=13, -11<=l<=14	-10<=h<=8, -18<=k<=18, -20<=l<=19	-10<=h<=10, -11<=k<=11, -14<=l<=14
Reflections collected	5658	12158	29633
Independent reflections	2654 [R(int) = 0.0504]	4061 [R(int) = 0.0191]	3275 [R(int) = 0.0376]
Reflections observed	2179	3601	3007
Completeness to theta	99.9 % to 25.242°	99.6 % to 67.684°	94.5 % to 67.684°
Max. and min. transmission	1.00000 and 0.82475	1.00000 and 0.90121	1.00000 and 0.79120
Data / restraints / parameters	2654 / 0 / 106	4061 / 2 / 281	3275 / 0 / 246
Goodness-of-fit on F^2	1.027	1.116	1.071
Final R indices [I>2sigma(I)]	R1 = 0.0462, wR2 = 0.1003	R1 = 0.0377, wR2 = 0.0990	R1 = 0.0415, wR2 = 0.1204
R indices (all data)	R1 = 0.0593, wR2 = 0.1076	R1 = 0.0448, wR2 = 0.1020	R1 = 0.0450, wR2 = 0.1250
Largest diff. peak and hole [$e.Å^{-3}$]	0.930 and -0.552	0.459 and -0.525	0.957 and -0.735
CCDC number	1017003	1017004	1017005

Compounds	$[Zn(LH_2)OTf_2]$ (**4**)	$[Zn_2(L)_2]$ (**5**)	$[Fe(LH)_2]\cdot H_2O$ (**6**)
Empirical formula	$C_{16}H_{16}F_6N_6O_6S_2Zn$	$C_{28}H_{28}N_{12}Zn_2$	$C_{28}H_{32}FeN_{12}O$
Formula weight	631.84	663.36	608.50
Wavelength [Å]	1.54184	1.54184	1.54184
Crystal system	Monoclinic	Monoclinic	Triclinic
Space group	C2/c	I2/a	P-1
a [Å]	14.6922(4)	15.3105(7)	8.2454(2)
b [Å]	10.5125(2)	12.1441(5)	11.0379(2)
c [Å]	17.3013(5)	15.6339(6)	16.9513(4)
α [°]	90	90	97.230(2)
β [°]	120.944(4)	92.310(4)	93.365(2)
γ [°]	90	90	110.444(2)
Volume [$Å^3$]	2291.88(13)	2904.5(2)	1425.33(6)
Z	4	4	2
Density (calculated) [Mg/m^3]	1.831	1.517	1.418
Absorption coefficient [mm^{-1}]	4.106	2.368	4.619
F(000)	1272	1360	636
Crystal size [mm^3]	0.13 x 0.1 x 0.06	0.13 x 0.11 x 0.07	0.35 x 0.2 x 0.1
Crystal description	yellow plate	red prism	dark brown plate
Theta range for data collection [°]	5.306 to 76.109	4.612 to 75.928	2.644 to 76.166
Index ranges	-18<=h<=18, -10<=k<=12, -21<=l<=21	-14<=h<=17, -15<=k<=15, -19<=l<=19	-10<=h<=10, -13<=k<=13, -20<=l<=19
Reflections collected	13446	12417	25820
Independent reflections	2320 [R(int) = 0.0189]	2945 [R(int) = 0.0379]	5513 [R(int) = 0.0457]
Reflections observed	2250	2702	4697
Completeness to theta	97.9 % to 67.684°	98.6 % to 67.684°	94.8 % to 67.684°
Max. and min. transmission	1.00000 and 0.83624	1.00000 and 0.68734	1.00000 and 0.55870
Data / restraints / parameters	2320 / 0 / 169	2945 / 0 / 192	5513 / 2 / 395
Goodness-of-fit on F^2	1.066	1.119	1.024
Final R indices [I>2sigma(I)]	R1 = 0.0313, wR2 = 0.0867	R1 = 0.0633, wR2 = 0.1761	R1 = 0.0485, wR2 = 0.1271
R indices (all data)	R1 = 0.0318, wR2 = 0.0871	R1 = 0.0661, wR2 = 0.1802	R1 = 0.0598, wR2 = 0.1352
Largest diff. peak and hole [$e.Å^{-3}$]	0.681 and -0.462	2.720 and -1.137	0.420 and -0.467
CCDC number	1017006	1017007	1017008